Stochastic Modeling for Studies of Real-World PHEV Usage: Driving Schedule and Daily Temporal Distributions

Tae-Kyung Lee, *Member, IEEE*, Zevi Bareket, Timothy Gordon, and Zoran S. Filipi, *Member, IEEE*

***Abstract*—Daily driving missions provide the fundamental information required to predict the impact of the plug-in hybrid electric vehicle (PHEV) on the grid. In this paper, we propose a statistical modeling approach of daily driving mission sets. The approach consists of temporal distribution modeling and the synthesis of individual representative cycles. The proposed temporal distribution model can capture departure and arrival time distributions with a small number of samples by statistically relating the distributions. Then, representative naturalistic cycles are constructed through a stochastic process and a subsequent statistical analysis with respect to driving distance. They are randomly assigned to the temporal distribution model to build up complete daily driving missions. The proposed approach enables the assessment of the impact on the grid of a large-scale deployment of PHEVs using a small number of simulations capturing real-world driving patterns and the temporal distributions of departure and arrival times.**

***Index Terms*—Daily driving mission, plug-in hybrid electric vehicle (PHEV), real-world driving, stochastic process, temporal distribution.**

I. Introduction

RECENT expansion of vehicle-to-grid (V2G) research requires relating vehicle-level studies to electric-grid studies. Realistic and representative daily driving missions are the key elements that set up the connection between plug-in hybrid electric vehicles (EVs) and the grid. Daily driving missions directly determine the electricity amount required by each plug-in hybrid EV (PHEV) from the grid and enable the planning of charging schedules for the best benefit. To predict the PHEV impact on the grid, extensive data are required. The data set could be up to several hundred thousand trips [1]. However, detailed PHEV simulation, which can predict the time histories of component responses under given driving schedules with sufficient accuracy, pushes the computational time beyond the manageable limits with such a large data set.

Manuscript received April 22, 2011; revised August 19, 2011 and November 14, 2011; accepted November 15, 2011. Date of publication December 22, 2011; date of current version May 9, 2012. This work was supported by the Department of Energy U.S.–China Clean Energy Research Center on Clean Vehicle Collaboration (CERC-CVC), University of Michigan. The review of this paper was coordinated by Prof. M. E. Benbouzid.

T.-K. Lee, T. Gordon, and Z. S. Filipi are with the Department of Mechanical Engineering, University of Michigan, Ann Arbor, MI 48109 USA (e-mail: kteel@umich.edu; tjgordon@umich.edu; filipi@umich.edu).

Z. Bareket is with the University of Michigan Transportation Research Institute, Ann Arbor, MI 48109 USA (e-mail: bareket@umich.edu).

Color versions of one or more of the figures in this paper are available online at http://ieeexplore.ieee.org.

Digital Object Identifier 10.1109/TVT.2011.2181191

Temporal distribution information of driving cycles is important to predict the PHEV impact on the electric power grid. Daily driving missions show wide spectrums in departure time, arrival time, driving patterns, driving distance, and locations [2], [3]. Accurate prediction of the amount of electricity consumption and battery state of charge is required for grid side planning, such as power grid asset management and emission control. Detailed PHEV simulation enables accurate prediction of vehicle operations [4], but running detailed simulations for studies of large fleets of vehicles is prohibitively expensive. Therefore, the prediction of PHEV electric load on the grid requires a novel approach capable of linking the vehicle usage data, including representative driving conditions and temporal distributions of vehicles at rest, with the electric energy consumption for a large sample size.

Construction of a model for relating the departure time distribution and the arrival time distribution is a new research topic in the PHEV and grid studies. Charging opportunity is highly connected to the PHEV arrival time when the main charging opportunity is the time before departure on the next day. If the arrival time distribution can be estimated from the departure time, the potential charging opportunity at home can be determined. Furthermore, the effort in collecting full daily driving schedule data to obtain the arrival time distribution is not necessary once the model is developed. Thus, the daily driving models, which relate the temporal distributions and the driving distance distribution, can reduce the number of simulation cases for the assessment of the PHEV impact on the grid and the development of charging scenarios. The reduced number of cases will enable the detailed vehicle level simulation.

Most of previous studies of PHEVs were focused on the design/optimization of PHEVs [5]–[7] and control design [8]–[11]. Driving patterns of individual trips were used as important factors in PHEV design/optimization in [5] and [6]. Temporal distribution of charging opportunity and driving cycles were considered in determining optimal battery size [7]. It was shown that the performance of the designed control in PHEVs is significantly affected by driving cycles [9]. PHEV power management strategies were investigated, accounting for driving cycles and variable energy price ratios in [10]. Recently, several studies related to the assessment of the environmental impacts of PHEVs were reported in [12] and [13]. The impact of PHEVs on utility system operations was evaluated through the simulation of a fleet of PHEVs under a variety of charging scenarios in [13].

In previous studies, PHEV energy consumption was predicted with constant specific electricity (in kilowatts per hour per mile), regardless of driving distances and patterns. Unrealistic assumption of constant specific electricity in the PHEV simulation will result in inaccurate prediction of the electric load. Many previous studies used certification driving cycles, such as Urban Dynamometer Driving Schedule (UDDS) and High Way Fuel Economy Test cycles, in evaluating vehicle performances [14], [15], although naturalistic driving cycles show a very different instantaneous load, compared with the certification cycles [2]–[4]. To reproduce the possible aggressiveness of real-world driving patterns, several scaled UDDS cycles were used in testing PHEVs [15], but not all real-world driving characteristics could be reproduced. Recent studies showed that the electricity requirement is highly dependent on driving distances [2], [4], [16], [17]. Therefore, the prediction accuracy can be further improved when representative real-world driving cycles, sensitive to the driving distance, are used in the PHEV simulation.

Driving cycle construction procedures have been developed over time to capture the naturalistic driving patterns. Various driving cycle development approaches are summarized by André in [18]. These approaches are grouped into two distinct categories: 1) Use on-road driving data in developing driving cycles, and 2) use a sequence of steady-speed and acceleration events to develop a contrived schedule. Many earlier driving cycle development efforts depend on random selections of driving segments [18]. Utilizing "microtrips" for constructing driving cycles proposed by Lin and Niemeier [19] relies on an iterative stochastic procedure, but sufficient representativeness of real-world patterns cannot be guaranteed due to subjective weightings in performance value evaluation. An alternative approach that utilizes Markov chain and transition probability matrices (TPMs) to capture features of naturalistic driving was proposed in [3] and further refined to improve the representativeness of synthetic cycles in [16] and [17]. This cycle synthesis approach is used to construct various distance driving cycles in this paper due to its flexibility in assigning arbitrary driving distances with the validated representativeness.

The objective of this paper is to propose a statistical modeling approach for generating daily driving missions. The generated daily vehicle missions include departure time and arrival time distributions, as well as representative real-world driving cycles. The relations between departure and arrival times were investigated first. The relations are modeled by analyzing the temporal distribution and the correlation between arrival and departure times. Then, synthetic driving cycles associated with the driving distance distribution are constructed. The synthetic cycles are subsequently assigned to the reproduced temporal distribution of trips, and daily vehicle usage schedules are obtained. Therefore, all aspects of the 24-h vehicle mission are captured in a compact way, thus providing a tool for assessing the effects of a large-scale PHEV or EV deployment without the need for processing a massive amount of data.

This paper is organized as follows: First, real-world data are analyzed, and the temporal distributions are investigated. Approaches to daily driving schedule construction are proposed in Section III. The constructed temporal distribution models are presented, and a driving synthesis approach utilizing stochastic models and subsequent statistical analysis follows in Section IV. Examples of the constructed one-day driving sets are presented in Section V. Finally, the findings are summarized in the conclusions.

II. Real-World Day Driving Schedule Data

A total of 830 days of driving that comprise 4409 trips and were analyzed from real-world driving data in Southeast Michigan, which is a typical region of the Midwest in the U.S., are used to extract driving information. The data were provided by the University of Michigan Transportation Research Institute (UMTRI) from the previously conducted field operational test (FOT) [20]. In their FOT, UMTRI outfitted 11 midsize vehicles (Nissan Altimas) with data acquisition systems. The data include the information of departure times, arriving times, and vehicle speed profiles versus time with 0.1-s sampling. From the time participants turned on the key to the time they turned off the key, all data including their instantaneous time and speed were recorded and logged as a separate trip. Each single trip covers a wide variety of driving distances from less than 1 mi up to 66.9 mi.

Daily driving missions consist of several individual trips and rest periods. The departure time is determined from outgoing trips from home, and the arrival time is determined from the last trip to home. However, the acquired data include consecutive driving events, and no information to separate daily driving is included. Thus, the start time of daily missions is determined by investigating the patterns of the start and end times of each trip. We assume that the longest rest times will separate each daily schedule, thus setting the threshold time for starting daily missions to 5 A.M. The threshold could be different, but the determined departure time distribution in Fig. 1(a) shows plausible results. The departure time distribution shows one high peak around 7–8 A.M., and the time window corresponds well to the general commuting times [20]. The departure time distribution is skewed to the left, the mean value is 10.53 (10:32 A.M.), and the standard deviation (std) is 3.26 h. In contrast, the arrival time distribution is not skewed and shows the Gaussianlike distribution with relatively small two peaks around 5:30 P.M. and 8:30 P.M. The trend in Fig. 1(b) suggests that people tend to randomly arrive at home and may have other trips after work. The mean value is 19.16 (7:10 P.M.), and the standard deviation is 3.62 h. We note that the standard deviations of the departure distribution and the arrival time distribution are relatively close, although the distribution profiles are different. Daily driving distance distribution is shown in Fig. 1(c). The daily driving distances are calculated by adding up all trip distances. The daily driving distance ranges from 1.51 to 137.2 mi. The mean value is 34.98 mi, and the standard deviation is 19.56 mi.

Fig. 2 shows the mean positive velocity distributions of a single trip. It shows clear dependence of the mean velocity on the driving distance. The mean positive velocity tends to increase along with the increasing driving distance. For short-distance trips (less than 9 mi), the mean value is 27.05 mi/h, and the standard deviation is 6.83 mi/h. The low speed implies that the short trips predominantly consist of local driving and frequent stops. In contrast, the mean of the mean positive

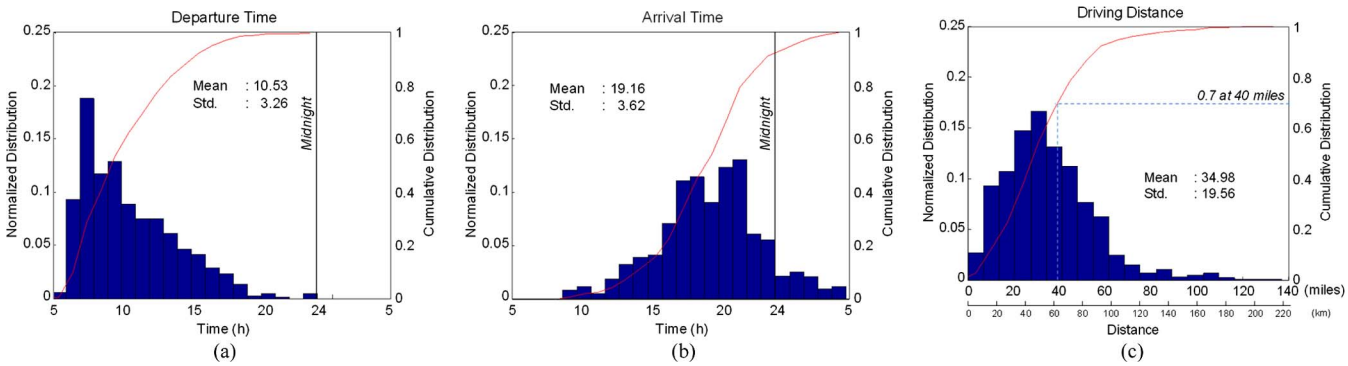

Fig. 1. Statistics of daily driving missions. (a) Departure time distribution. (b) Arrival time distribution. (c) Driving distance distribution.

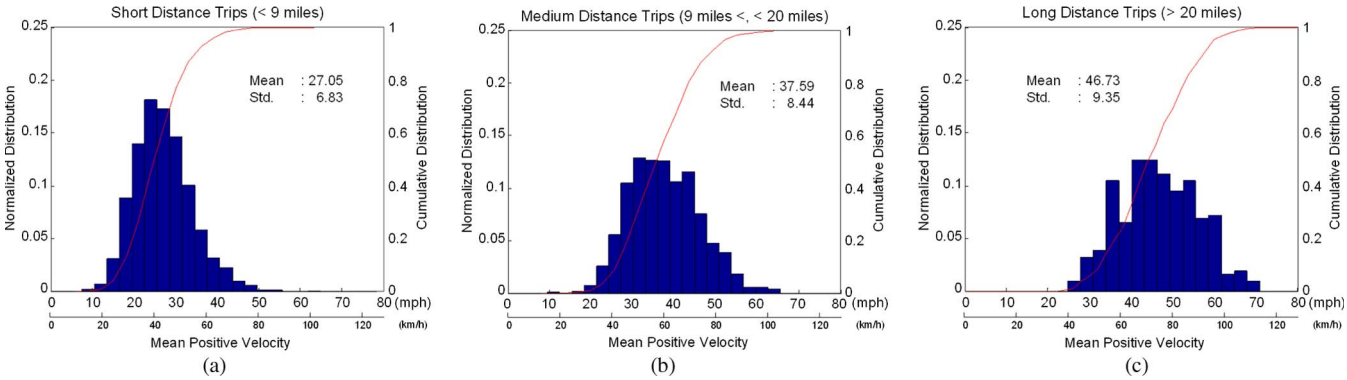

Fig. 2. Histograms and cumulative probability plots of mean positive velocity with respect to driving distances. (a) Short-distance trips (shorter than 9 mi). (b) Medium-distance trips (longer than 9 mi but shorter than 20 mi). (c) Long-distance trips (longer than 20 mi).

velocity of long trips is 46.73 mi/h, and its maximum is 71.06 mi/h. In the extreme case with maximum mean velocity, the trip mainly consists of freeway driving. In general, the trips include both local and freeway driving in most cases.

The correlations between the driving distance and the departure/arrival time distribution are investigated next. The daily driving distance distributions with respect to the departure time and the arrival time are shown in Fig. 3. No clear relationships between driving distances and other indices are shown. The correlation is quantified by the β value defined as $\mathrm{Cov}(y,x)/\mathrm{Var}(x)$, where $\mathrm{Cov}(y,x)$ is the covariance between variables y and x, and $\mathrm{Var}(x)$ is the variance of variable x. The value for β ranges from -1 to 1, and if two variables are not correlated at all, i.e., completely independent each other, the value of β is zero. Thus, the daily driving distance can be assumed to be independent of the departure time and the arrival time with small $|\beta|$ values. Fig. 3 shows the distributions; therefore, the driving distance is considered as an independent variable with respect to the departure time and the arrival time. The independence makes the daily driving schedule modeling simpler.

The distribution of arrival time versus departure time is shown in Fig. 4. If the arrival time distribution can be reproduced from the departure time distribution, only departure time information is required to predict the entire temporal distribution of daily driving missions. Thus, the temporal distribution can be reproduced with a relatively small number of cases. Reproducing this distribution using stochastic models is the main objective of this paper.

III. Stochastic Model of Daily Schedule Sets

A daily schedule model is constructed based on statistical approaches derived from the observation of real-world driving data. The model consists of two parts: 1) temporal distribution models of the departure time and the arrival time and 2) synthesized representative driving cycles for the given driving distances.

A. Temporal Distribution Model

Temporal distributions of the departure time and the arrival time of daily missions are correlated through a stochastic modeling approach. The arrival time distribution is dependent on the departure time distribution. Thus, the arrival time distribution at a concerning departure time is expressed as a conditional probability. In this model, the arrival time distribution at each concerning departure time window is expressed as

$$P_{\mathrm{ARR}}(t_{\mathrm{arr}}) = \sum_{i=1}^{N} P_{\mathrm{ARR,DEP}}(t_{\mathrm{arr}} \mid t_{\mathrm{dep},i}) f_{\mathrm{DEP}}(t_{\mathrm{dep},i}) \quad (1)$$

where $P_{\mathrm{ARR}}(t_{\mathrm{arr}})$ is the probability density function (pdf) of the arrival time t_{arr}, $f_{\mathrm{DEP}}(t_{\mathrm{dep},i})$ is the probability mass function (pmf) of the ith departure time window $t_{\mathrm{dep},i}$, N is the number of the discrete departure time window, $P_{\mathrm{ARR,DEP}}(t_{\mathrm{arr}}|t_{\mathrm{dep},i})$ is the conditional pdf of arrival time t_{arr} on $t_{\mathrm{dep},i}$. $f_{\mathrm{DEP}}(t_{\mathrm{dep},i})$ is obtained from the integral

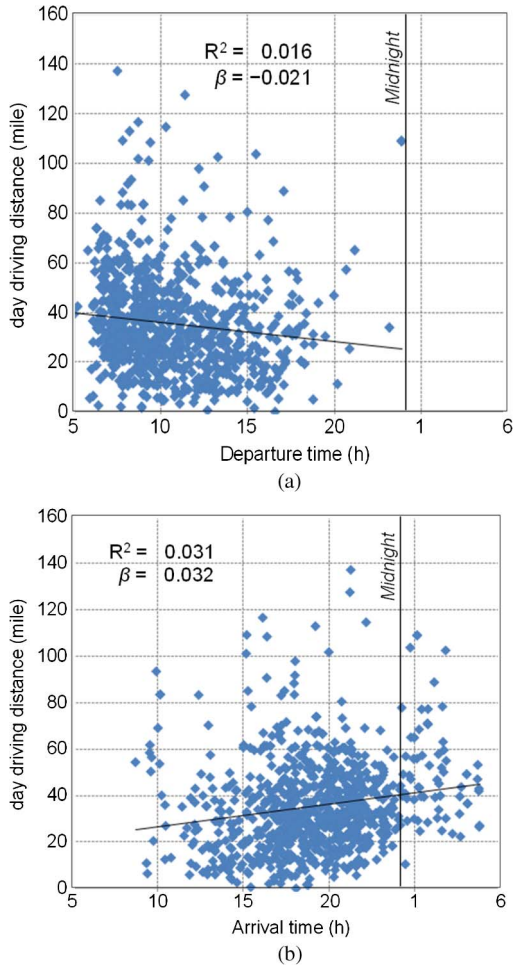

Fig. 3. Day driving distance distributions with respect to (a) departure time and (b) arrival time.

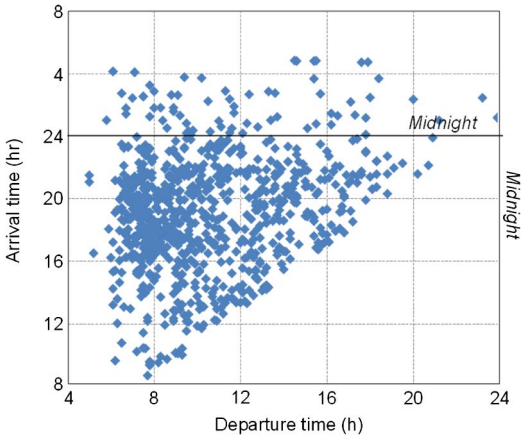

Fig. 4. Temporal distribution of the departure and arrival times over 24 h.

of the $P_{\mathrm{DEP}}(t_{\mathrm{dep}})$ over the range of $(t_{\mathrm{dep},i,\mathrm{lb}}, t_{\mathrm{dep},i,\mathrm{ub}}]$ and expressed as

$$f_{\mathrm{DEP}}(t_{\mathrm{dep},i}) = \int_{t_{\mathrm{dep},i,lb}}^{t_{\mathrm{dep},i,\mathrm{ub}}} P_{\mathrm{DEP}}(t_{\mathrm{dep}})dt_{\mathrm{dep}} \tag{2}$$

where $P_{\mathrm{DEP}}(t_{\mathrm{dep}})$ is the pmf of the departure time t_{dep}.

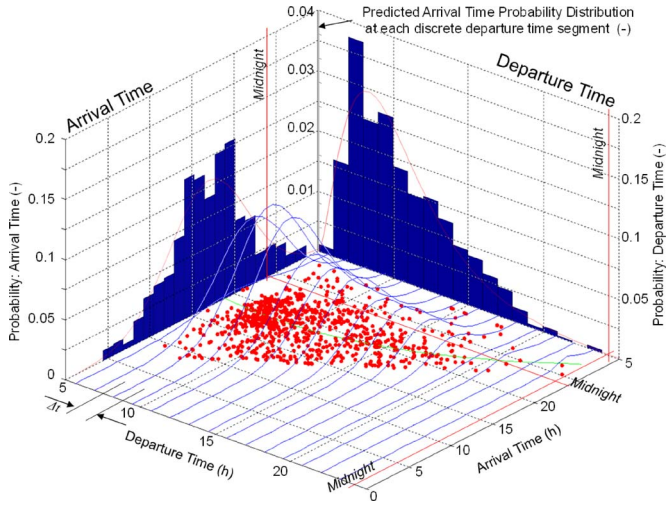

Fig. 5. Conceptual illustration of the departure and arrival time temporal distribution model.

The departure time pmf satisfies

$$\sum_{i=1}^{N} f_{\mathrm{DEP}}(t_{\mathrm{dep},i}) = 1 \tag{3}$$

and the arrival time pdf satisfies

$$\int_{\mathrm{OneDay}} P_{\mathrm{APR}}(t_{\mathrm{arr}})dt_{\mathrm{arr}} = 1. \tag{4}$$

The departure time and arrival time distribution model is shown in Fig. 5. From (1), the arrival time distribution is obtained by the sum of the arrival time distributions at each departure time window. In this paper, the departure time distribution is modeled in the form of chi-square distribution (χ^2-distribution)

$$f_{\mathrm{DEP}}(t_{\mathrm{depn},i}) = \frac{t_{\mathrm{depn},i}^{(\nu-2)/2} e^{-t_{\mathrm{depn},i}/2}}{2^{v/2}\Gamma(v/2)} \tag{5}$$

where $\Gamma(.)$ is the Gamma function defined as $\Gamma(z) = \int_0^\infty t^{z-1}e^{-1}dt$, $t_{\mathrm{depn},i}$ is the normalized departure time at the ith departure time window and defined as $t_{\mathrm{dep},i}/\Delta t$, and Δt is the discretized window size.

ν is determined to minimize the root-mean-square error of the response variable by applying sequential quadratic programming. Although the chi-square distribution function has its own interpretation, we only use the structure to find the best regression. The regression equation follows the real-world data distribution well, as shown in Fig. 5.

The arrival time pdf is determined in the form of Gaussian distribution at each departure time window. Fig. 6 shows the procedure of the arrival time distribution prediction. The arrival time distribution at the ith departure time window is assumed as the Gaussian distribution (i.e., normal distribution) and expressed as

$$P_{\mathrm{ARR,DEP}}(t_{\mathrm{arr}} \mid t_{\mathrm{dep},i}) = \frac{1}{\sqrt{2\pi\sigma_i^2}} e^{-\frac{(t_{\mathrm{arr}}-\mu_i)^2}{2\sigma_i^2}} \tag{6}$$

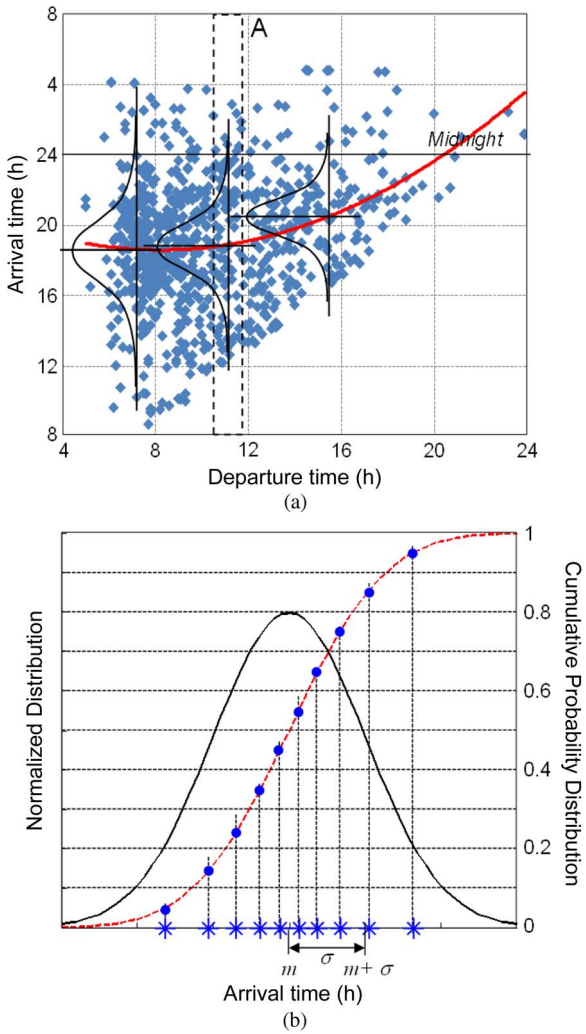

Fig. 6. Arrival time distribution models. (a) Conceptual illustration. (b) Example of the arrival time distribution model represented by the Gaussian distribution.

where μ_i is the mean of the arrival time at the ith departure time window, and σ_i is the standard deviation of the arrival time at the ith departure time window. The mean and the standard deviation of the arrival time at each departure time window are regressed to capture the trend of arrival time distributions [see Fig. 6(a)]. Then, the mean and the standard deviation of the arrival time are used to model the arrival time distribution in each departure time window. The arrival time distribution is obtained through the inversion of the normal probability [see Fig. 6(b)], i.e.,

$$t_{\text{arr}} = \left(\Phi^{-1}\left([j-0.5]/n_i\right), \qquad \text{for } j = 1, \ldots, n_i \tag{7}$$

where Φ is the cumulative distribution function (cdf) of the normal distribution of the arrival time in the concerning departure time window, and n_i is the number of arrival time samples in the ith departure time window.

The arrival time distribution computed from (1) is shown in Fig. 5. The constructed probability distribution of the arrival time is well matched to the histogram of arrival time, although the Gaussian distribution assumption of the arrival time distribution may not be valid in some departure time windows.

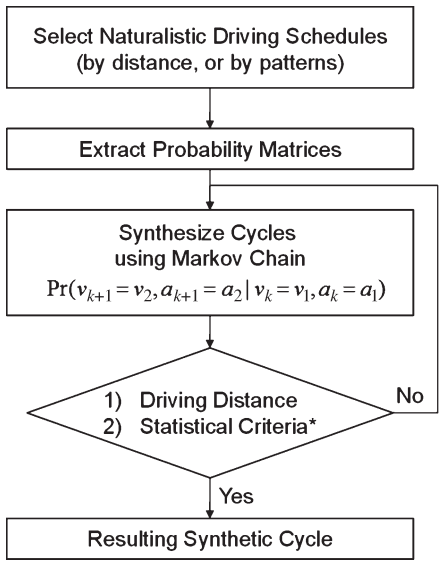

Fig. 7. Naturalistic driving cycle synthesis procedure using Markov chain and statistical criteria.

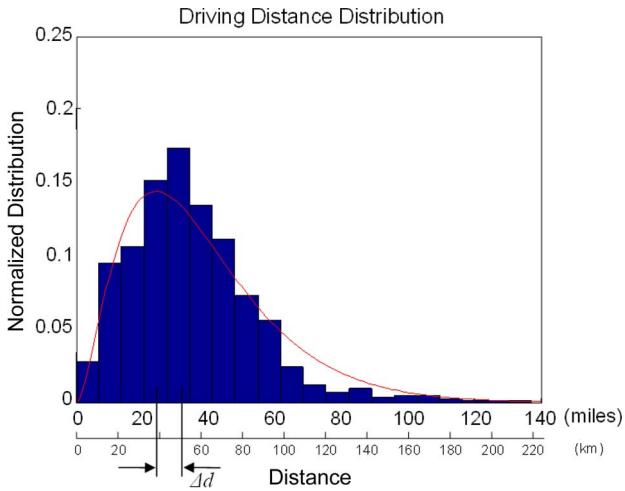

Fig. 8. Statistical distribution of daily driving distances: probability density function, cumulative density function, and selection of driving distance for synthetic cycles with the same probability, depending on the driving distances.

B. Driving Cycle Synthesis Procedure

Representative synthetic driving cycles are constructed using a stochastic process and statistical analyses. The representativeness of the constructed cycles is assessed by comparing their statistically significant variables to the reference real-world values. The synthesis procedure proposed by Lee and Filipi [16] is used to construct synthetic cycles at given trip distances. The overall procedure is shown in Fig. 7 and briefly introduced here for the readers' convenience.

While synthesizing driving cycles, the Markov chain is used as a stochastic procedure due to its relative simplicity in representing an unknown system and its flexibility in constructing cycles. A discrete-time Markov chain is a sequence of random variables $X_1, X_2, X_3, \ldots$, with the Markov property expressed as

$$P(X_{n+1} = x_{n+1} | X_1 = x_1, X_2 = x_2, \ldots, X_n = x_n) = P(X_{n+1} = x_{n+1} | X_n = x_n). \tag{8}$$

TABLE I
POSSIBLE 27 EXPLANATORY VARIABLES AND NOMINATED 16 EXPLANATORY VARIABLES FOR THE INITIAL REGRESSION ANALYSIS

Category	Initial possible explanatory variables	Nominated explanatory variables
Velocity related variables	1) Mean positive velocity (mph) 2) Mean velocity (mph): include zero velocity 3) Maximum velocity (mph) 4) 95% maximum velocity (mph) 5) Standard deviation of velocity (mph)	1) Mean positive velocity (mph) 2) Standard deviation of velocity (mph)
Acceleration related variables	6) Mean positive acceleration (m/sec^2) 7) Mean negative acceleration (m/sec^2) 8) Positive acceleration time (sec) 9) Negative acceleration time (sec) 10) 95% maximum positive acceleration (m/sec^2) 11) 95% minimum negative acceleration (m/sec^2) 12) Maximum acceleration (m/sec^2) 13) Minimum acceleration (m/sec^2) 14) Standard deviation of acceleration (m/sec^2) 15) Percentage of driving time under positive acceleration (%) 16) Percentage of driving time under negative acceleration (%)	3) Mean positive acceleration (m/sec^2) 4) Mean negative acceleration (m/sec^2) 5) Maximum acceleration (m/sec^2) 6) Minimum acceleration (m/sec^2) 7) Standard deviation of acceleration (m/sec^2) 8) Percentage of driving time under positive acceleration (%) 9) Percentage of driving time under negative acceleration (%)
Driving distance and time	17) Driving distance (mile) 18) Driving time (sec)	10) Driving distance (mile) 11) Driving time (sec)
Driving characteristics	19) Idle time (sec) 20) Percentage of idle time (%) 21) Cruise time (sec) 22) Percentage of cruise time (%) 23) Number of stops ( ) 24) Number of stops/mile (/mile) 25) Mean specific power (W/mile) 26) Maximum specific power (W/mile) 27) Minimum specific power (W/mile)	12) Percentage of idle time (%) 13) Percentage of cruise time (%) 14) Number of stops/mile (/mile) 15) Maximum specific power (W/mile) 16) Minimum specific power (W/mile)

The random variables X_n are called the state space of the chain. The conditional probabilities $p_{ij} := P(X_{n+1} = j | X_n = i)$ are called transition probabilities, and they satisfy

$$\sum_j p_{ij} = \sum_j P(X_{n+1} = j | X_n = i) = 1. \tag{9}$$

The driving cycle information is extracted from the real-world driving data in the form of TPMs with two states, i.e., velocity and acceleration. The states are selected from the vehicle dynamic equation to describe vehicle behavior, and the dynamic equation is expressed as

$$F_{\text{net}} = F_{\text{prop}} - F_{\text{RR}} - F_{\text{WR}} - F_{\text{GR}} = m_e a_{\text{veh}} = m_e \dot{v}_{\text{veh}} \tag{10}$$

where F_{net} is the net force applied to the vehicle, F_{prop} is the propulsion force from the powertrain, F_{RR} is the rolling resistance force, F_{WR} is the wind resistance force, F_{GR} is the grade resistance force and all external forces applied to the vehicle, m_e is the equivalent vehicle mass, v_{veh} is the vehicle velocity, and a_{veh} is the vehicle acceleration. The TPM is generated in the form of a 2-D matrix with velocity and acceleration at current time t_k, and the conditional probability is expressed as

$$P(v_{k+1} = v_2, a_{k+1} = a_2 \mid v_k = v_1, a_k = a_1) \tag{11}$$

at a given cycle velocity v_1 and acceleration a_1.

The data are divided into ten different bins having the same probability on the cdf. The ten divisions can capture different driving patterns with respect to driving distances. Candidate representative driving cycles are synthesized using the Markov chain, and the cycle that satisfies the significant statistical criteria is deemed representative. The representative driving distances in each bin are selected as the median cumulative distribution in each bin. The probability distribution of the driving distance is regressed with the form of the χ^2-distribution, i.e.,

$$P_{\text{DIST}}(x_{i,n}) = \frac{x_{i,n}^{(\nu-2)/2} e^{-x_{i,n}/2}}{2^{\nu/2}\Gamma(\nu/2)} \tag{12}$$

where $x_{i,n}$ is the normalized driving distances defined as $x_i/\Delta d$, x_i is the mean driving distance in the ith driving distance window, and Δd is the discretized window size in Fig. 8.

The statistical criteria for assessing the representativeness of cycles are determined through a generalized linear regression analysis with the response variable of the power intensity defined as the specific power at the wheels per mile. The overall procedure to determine the statistical criteria is briefly described as follows: Initially, a total of 27 possible explanatory variables are identified [16] and categorized into velocity-related, acceleration-related, driving-time- and distance-related, and event-related variables. When two variables show clear relationship, one of them is removed from the nominated variables. Thus, 16 variables are nominated as initial explanatory variables for the regression analysis, as shown in Table I. Then, the regression analysis is executed and assessed using the normal probability plots of the residuals and the histogram of the residuals. The least significant variable is dropped based on *t-test* results, whereas the resulting equations are good enough to represent the response variable. The final regression equations determine statistically significant variables to assess the representativeness of synthesized driving cycles, and the variables are given as follows:

1) standard deviation of velocity (in miles per hour);
2) mean positive acceleration (in meters per square second);
3) standard deviation of acceleration (in meters per square second);

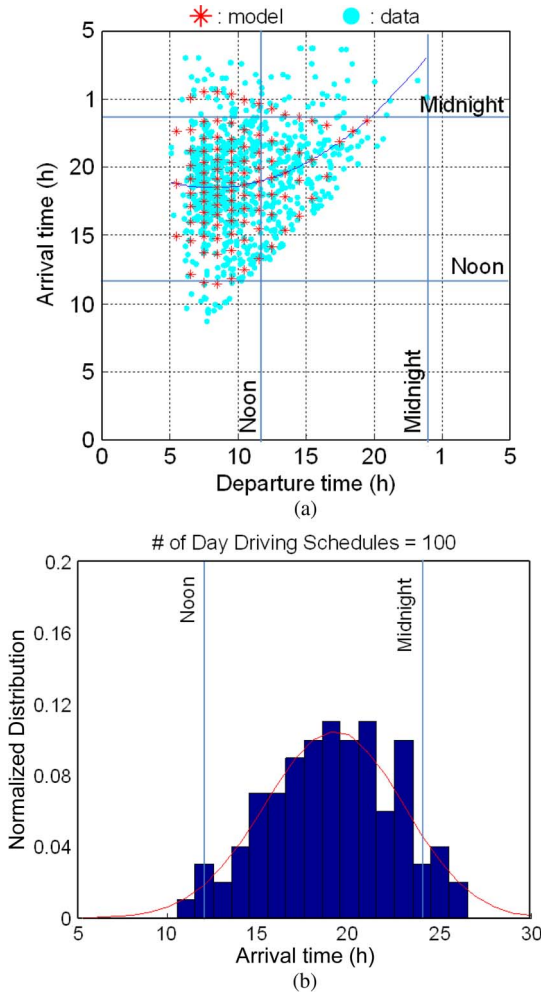

Fig. 9. Constructed temporal distribution of the departure and arrival times with 100 daily missions. (a) Comparison between real-world data and the constructed distribution. (b) Histogram of the constructed distribution of the arrival time.

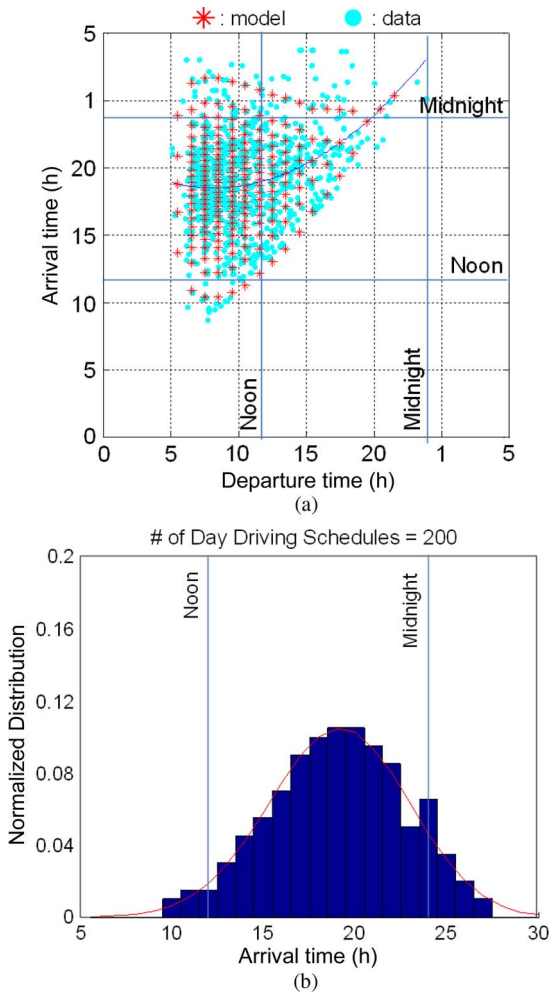

Fig. 10. Constructed temporal distribution of the departure and arrival times with 200 daily missions. (a) Comparison between real-world data and the constructed distribution. (b) Histogram of the constructed distribution of the arrival time.

4) percentage of driving time under positive acceleration (in percent);
5) percentage of driving time under negative acceleration (in percent);
6) mean positive velocity (in miles per hour);
7) percentage of idle time (in percent);
8) number of stops per mile (1/mi).

IV. Daily Mission Set Synthesis

Daily schedule sets are constructed accounting for the departure and arrival time temporal distributions, and the driving distance distribution. The constructed daily schedule sets reproduce the temporal distributions with a reduced number of cases. The arrival time distribution is predicted from the departure time distribution using the proposed model. The number of trips is determined to make the arrival time distribution close to the measured data set. When the total number of trips N is given, the number of day trips in the ith departure time window is calculated from

$$n_i = N f_{\mathrm{DEP}}(t_{\mathrm{dep},i}) = N \int_{t_{\mathrm{dep},i}}^{t_{\mathrm{dep},i+1}} P(t_{\mathrm{dep}}) dt_{\mathrm{dep}} \qquad (13)$$

where $f_{\mathrm{DEP}}(t_{\mathrm{dep},i})$ is the pmf of the ith departure time window $t_{\mathrm{dep},i}$ expressed in (2). Then, the arrival time distribution in the ith departure time window is determined from the inverse normal probability function in (8).

The constructed temporal distributions are validated through the comparison with the measured original distribution. Figs. 9 and 10 show two different cases with 100 and 200 daily missions, respectively. The constructed distributions are overlapped on the regressed distribution from the real-world data. With a relatively small number of missions (100 missions), the resulting arrival time distribution shows slight roughness but captures the overall distribution trend, as shown in Fig. 9(b). The temporal distribution in Fig. 9(a) also shows good visual correspondence to the measured data. We note that a small number of missions may not be sufficient to capture the arrival time distribution. In contrast, when the number of points becomes large, the constructed arrival distribution is much smoother and follows well the reference probability curve, as shown in Fig. 10(b).

The daily schedule set is completed by randomly assigning synthetic driving cycles to the temporal distribution, with the assumption that driving distance is independent of the temporal

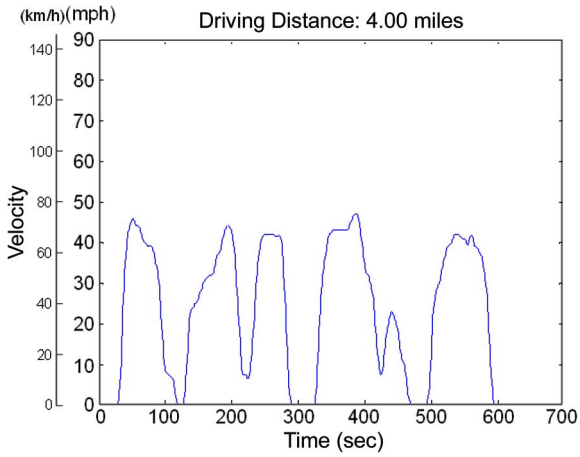

Fig. 11. Synthesized naturalistic driving cycles using real-world driving cycle data around the driving distance of 4.0 mi.

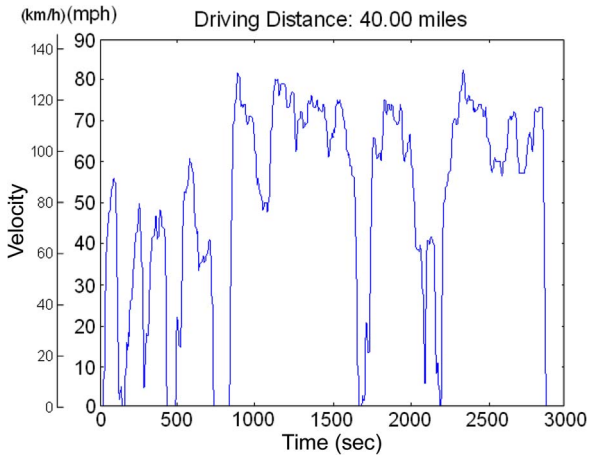

Fig. 12. Synthesized naturalistic driving cycles using real-world driving cycle data around the driving distance of 40.0 mi.

distribution of the departure and arrival times, as discussed in Section II. The only constraint while assigning the synthetic cycle is that the cycle duration must be shorter than the duration between the departure time and the arrival time. The same numbers of driving cycles to the schedule set satisfying the driving distance distribution in Fig. 8 are synthesized. Figs. 11 and 12 show two examples of the representative synthetic cycles in the shortest distance bin and in the longest distance bin, respectively. The values of the statistical parameters are compared in Tables II and III, and they show good agreement. In the synthetic cycles, the driving patterns are quite different at short- and long-distance cycles. The mean velocity of the long-distance cycle (54.59 mi/h) is almost twice that of the short-distance case (28.75 mi/h). The number of stops per mile (0.99) is almost seven times many at the short-distance trip (0.15). The driving patterns over a longer distance become more aggressive, with a maximum velocity of more than 80 mi/h and significant driving periods at more than 60 mi/h.

Fig. 13 shows the resulting one-day driving set consisting of 200 daily missions. Although the resulting driving set is simple, compared with the real cases, it is valuable to evaluate the charging scenario when vehicles are charged mainly overnight. Fig. 13(b) shows one example of the constructed daily driving set at the departure time window with the departure time of 8:30 A.M. The resulting missions include both temporal distribution and detailed driving velocity profiles. Thus, the detailed vehicle level analysis can be directly connected to the grid side studies.

TABLE II
COMPARISON OF THE STATISTICAL PARAMETERS OF THE SYNTHETIC DRIVING CYCLE FOR THE DRIVING DISTANCE OF 4.0 mi

Statistical parameters	Real Cycles*	Synthetic Cycle
Distance (mile)	4	4.02
Mean pos. vel. (mph)	27.48	28.75
std. vel. (mph)	17.11	17.05
Mean pos. acc. (m/s^2)	0.99	1.03
std. acc. (m/s^2)	1.28	1.21
# stops/mile (1/mile)	1.04	0.99

* Mean values are presented for real cycles

TABLE III
COMPARISON OF THE STATISTICAL PARAMETERS OF THE SYNTHETIC DRIVING CYCLE FOR THE DRIVING DISTANCE OF 40.0 mi

Statistical parameters	Real Cycles*	Synthetic Cycle
Distance (mile)	40	40.26
Mean pos. vel. (mph)	52.16	54.59
std. vel. (mph)	24.68	24.93
Mean pos. acc. (m/s^2)	0.56	0.61
std. acc. (m/s^2)	0.92	0.84
# stops/mile (1/mile)	0.19	0.15

* Mean values are presented for real cycles

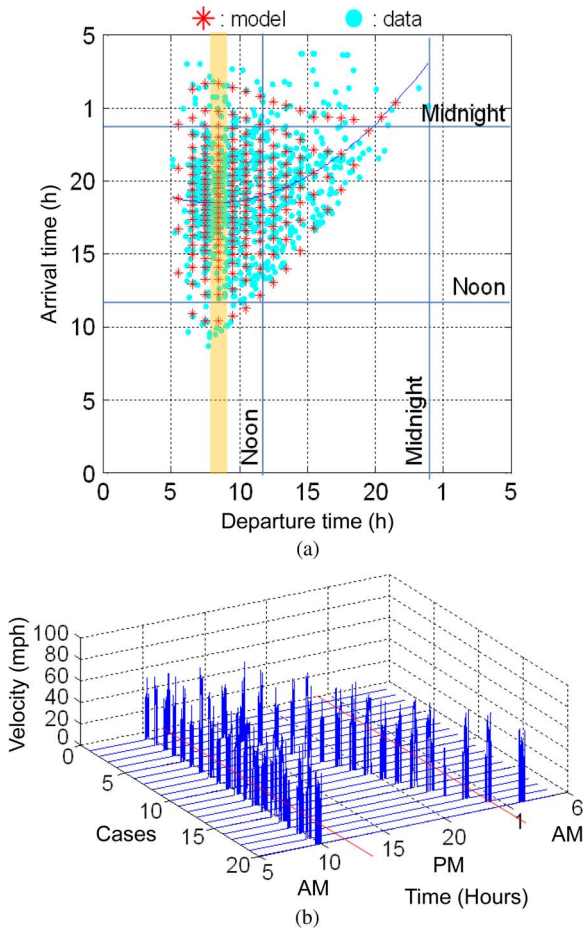

Fig. 13. One-day driving set with 200 daily missions. (a) Temporal distribution of the departure and arrival times. (b) One-day driving schedule subset with the departure time of 8:30 A.M.

V. Conclusion

The daily schedule modeling approach that reproduces the temporal distributions and the representative driving patterns with respect to driving distance has been proposed to reduce the simulation cases needed to cover the total number of real-world daily missions. The proposed approach consists of temporal distribution modeling and the synthesis of individual representative driving cycles. The temporal distribution model captures the vehicle departure and arrival time distributions with a small number of samples. Representative real-world cycles for capturing naturalistic driving patterns with respect to the driving distance have been constructed through a stochastic process and a subsequent statistical analysis with respect to driving distance. The constructed cycles have been randomly assigned to the resulting temporal distribution with a given number of samples.

The constructed daily driving sets have shown good agreement with the complete set of real-world data. The small number of cycles in the constructed one-day driving and vehicle resting schedules enables detailed PHEV simulation with manageable computational effort. The resulting integrated stochastic model allows PHEV design optimization and control design, as well as infrastructure-level studies, such as understanding of the interactions between the transportation sector and the power grid and the overall environmental impact.

References

[1] U.S. Dept. Transp. Bureau of Transp. Statist., *Highlight of the 2001 National Household Travel Survey*, 2001.

[2] B. Adornato, R. Patil, Z. Filipi, Z. Bareket, and T. Gordon, "Characterizing naturalistic driving patterns for Plug-in Hybrid Electric Vehicle analysis," in *IEEE VPPC 2009*, Ann Arbor, MI, 2009, pp. 655–660.

[3] B. Adornato, "Characterization of driving cycles for plug-in hybrid vehicles," M.S. thesis, Dept. Mech. Eng., Univ. Michigan, Ann Arbor, MI, 2009.

[4] T.-K. Lee and Z. S. Filipi, "Simulation based assessment of plug-in hybrid electric vehicle behavior during real-world 24-hour missions," presented at the SAE World Congr. Exhib., Detroit, MI, 2010, SAE Paper 2010-01-0827.

[5] R. Patil, B. Adornato, and Z. S. Filipi, "Impact of naturalistic driving patterns on PHEV performance and system design," presented at the SAE Powertrains Fuels Lubricants Meeting, San Antonio, TX, 2009, SAE Paper 2009-01-2715.

[6] R. Patil, B. Adornato, and Z. S. Filipi, "Design optimization of a series plug-in hybrid electric vehicle for real-world driving conditions," presented at the SAE World Congr. Exhib., Detroit, MI, 2010, SAE Paper 2010-01-0840.

[7] E. Tara, S. Shahidinejad, S. Filizadeh, and E. Bibeau, "Battery storage sizing in a retrofitted plug-in hybrid electric vehicle," *IEEE Trans. Veh. Technol.*, vol. 59, no. 6, pp. 2786–2794, Jul. 2010.

[8] P. B. Sharer, A. Rousseau, D. Karbowski, and S. Pagerit, "Plug-in hybrid electric vehicle control strategy: comparison between EV and charge-depleting options," presented at the SAE World Congr. Exhib., Detroit, MI, 2008, SAE Paper 2008-01-0460.

[9] S. G. Wirasingha and A. Emadi, "Classification and review of control strategies for plug-in hybrid electric vehicles," *IEEE Trans. Veh. Technol.*, vol. 60, no. 1, pp. 111–122, Jan. 2011.

[10] S. J. Moura, H. K. Fathy, D. S. Callaway, and J. L. Stein, "A stochastic optimal control approach for power management in plug-in hybrid electric vehicles," *IEEE Trans. Control Syst. Technol.*, vol. 19, no. 3, pp. 545–555, May 2011.

[11] B. Zhang, C. C. Mi, and M. Zhang, "Charge-depleting control strategies and fuel optimization of blended-mode plug-in hybrid electric vehicles," *IEEE Trans. Veh. Technol.*, vol. 60, no. 4, pp. 1516–1525, May 2011.

[12] T. Bevis, B. Hacker, C. S. Edrington, and S. Azongha, "A review of PHEV grid impacts," in *Proc. NAPS*, Starkville, MS, 2009, pp. 1–6.

[13] K. Parks, P. Denholm, and T. Markel, "Costs and emissions associated with plug-in hybrid electric vehicle charging in the xcel energy colorado service territory," Nat. Renewable Energy Lab., Golden, CO, Tech. Rep. NREL/TP-640-41410, May 2007.

[14] R. B. Carlson, H. Lohse-Busch, M. Duoba, and N. Shidore, "Drive cycle fuel consumption variability of plug-in hybrid electric vehicle due to aggressive driving," presented at the SAE World Congr. Exhib., Detroit, MI, 2009, SAE Paper 2009-01-1335.

[15] M. Duoba, R. B. Carlson, and D. Bocci, "Calculating results and performance parameters for PHEVs," Detroit, MI, 2009, SAE Paper 2009-01-1328.

[16] T.-K. Lee and Z. S. Filipi, "Synthesis of real-world driving cycles using stochastic process and statistical methodology," *Int. J. Veh. Design*, vol. 57, no. 1, pp. 17–36, 2011.

[17] T.-K. Lee and Z. S. Filipi, "Synthesis and validation of representative real-world driving cycles for plug-in hybrid vehicles," in *Proc. IEEE VPPC*, Lille, France, 2010, pp. 1–6.

[18] M. André, "Driving cycles development: Characterization of methods," presented at the Int. Fuels Lubricants Meeting Expo., Dearborn, MI, 1996, SAE Paper 961 112.

[19] J. Lin and D. A. Niemeier, "An exploratory analysis comparing a stochastic driving cycle to California's regulatory cycle," *Atmosp. Environ.*, vol. 36, no. 38, pp. 5759–5770, Dec. 2002.

[20] LeBlanc, J. Sayer, C. Winkler, R. Ervin, S. Bogard, J. Devonshire, M. Mefford, M. Hagan, Z. Bareket, R. Goodsell, and T. Gordon, "Road departure crash warning system field operational test: Methodology and results," Univ. Michigan, Transp. Res. Inst. (UMTRI), Ann Arbor, MI, Tech. Rep. UMTRI-2006-9-2, 2006.

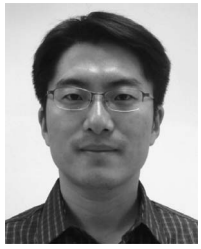

Tae-Kyung Lee (M'11) received the B.S. and M.S. degrees from Seoul National University, Seoul, Korea, in 1996 and 1998, respectively, and the Ph.D. degree from the University of Michigan, Ann Arbor, in 2009, all in mechanical engineering.

He is currently an Assistant Research Scientist with the Department of Mechanical Engineering, University of Michigan. He was a Senior Research Engineer with Hyundai Motor Company, Korea, from 1998 to 2005. His research interests include physical system modeling, optimization and control of advanced powertrains, optimization of hybrid propulsion system architecture, control design of hybrid propulsion systems, driving cycle analysis and synthesis, and battery modeling and analysis.

Dr. Lee received the Donald Julius Groen Award from the Institution of Mechanical Engineers Mechatronics, Informatics, and Control Group in 2011.

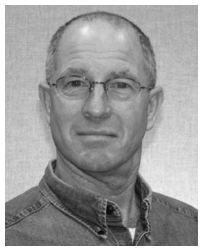

Zevi Bareket received the M.Sc. degree in mechanical engineering from the University of Michigan, Ann Arbor, in 1989.

He is currently a Senior Research Area Specialist with the University of Michigan Transportation Research Institute, Ann Arbor. He has published and coauthored numerous peer-reviewed journal papers, as well as conference presentations. His research interests are investigating intelligent transportation system (ITS) technologies aimed at enhancing highway safety and operations, as well as the development of driver models that represent the human operator. He has been involved with studies that addressed ITS approaches for collision avoidance of passenger vehicles and rollover prevention of heavy trucks. He is currently involved in ITS-related projects whose goal is to evaluate safety and performance of ITS technologies and to expand the understanding of the driving process. These technologies include both onboard systems such as adaptive control and crash warning, as well as roadside video monitoring systems.

Timothy Gordon received the B.A. degree in applied mathematics and the Ph.D. degree in theoretical physics from the University of Cambridge, Cambridge, U.K., in 1975 and 1978, respectively.

He is currently a Research Professor with the Department of Mechanical Engineering, University of Michigan, Ann Arbor. He is currently the Committee Chair for Vehicle-Highway Automation, Transportation Research Board of the National Academies of Science, Washington DC. He was Head of the Vehicle Systems and Control Group, University of Michigan Transportation Research Institute, and a Ford Professor of automotive engineering with Loughborough University, Leicestershire, U.K. He has 25 years of experience working on basic and applied research in mathematics, statistics, and engineering and has published more than 100 refereed papers. Much of his research has been with the automotive industry, including government sponsorship. His research interests include vehicle dynamics and control, adaptive and intelligent systems, and driver modeling, with special emphasis on active safety systems. Recently, he has developed new methods for evaluating safety benefits for electronically controlled safety systems under the U.S. Department of Transportation's Advanced Collision Avoidance Technologies Program.

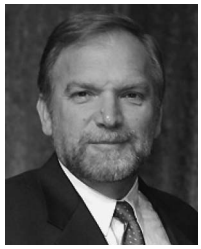

Zoran S. Filipi (M'10) received the M.S. and Ph.D. degrees in mechanical engineering from the University of Belgrade, Belgrade, Serbia, in 1987 and 1992, respectively.

He joined the University of Michigan, Ann Arbor, in 1994. He is currently a Research Professor of mechanical engineering with the Department of Mechanical Engineering, University of Michigan, Director of the Center for Engineering Excellence through Hybrid Technology, and a Faculty Fellow of the University of Michigan Energy Institute. He is currently the Associate Editor of the *ASME Journal of Engineering for Gas Turbines and Power*. His efforts on simulation and analysis of hybrid propulsion systems focus on architecture, design and control of electric and hydraulic hybrid powertrains, and powertrain-in-the-loop integration. He has published more than 120 papers in international journals and refereed conference proceeding papers. His research interests are advanced integrated circuit engine combustion concepts, alternative powertrains, and energy for transportation.

Dr. Filipi is a Society for Automotive Engineering (SAE) Fellow and a member of the SAE Executive Committee for Powertrains. He assumed the new position of Timken Endowed Chair for Vehicle System Design and Development with the Clemson University International Center for Automotive Research, Clemson, SC, in January 2012. He has received the SAE Forest R. McFarland Award, the IMechE Donald Julius Groen Award, and the University of Michigan Research Faculty Achievement Award.